Available online at www.sciencedirect.com

ScienceDirect

Green Energy & Environment xxx (xxxx) xxx

www.keaipublishing.com/gee

Research Paper

Piezoelectric-enhanced n-TiO_2/$BaTiO_3$/p-TiO_2 heterojunction for highly efficient photoelectrocatalysis

Minhua Ai [a,b,d], Zihang Peng [a,b,d], Xidi Li [a], Faryal Idrees [c], Xiangwen Zhang [a,b,d], Ji-Jun Zou [a,b,d], Lun Pan [a,b,d,*]

[a] *Key Laboratory for Green Chemical Technology of the Ministry of Education, School of Chemical Engineering and Technology, Tianjin University, Tianjin 300072, China*

[b] *Collaborative Innovative Center of Chemical Science and Engineering (Tianjin), Tianjin 300072, China*

[c] *Department of Physics, University of the Punjab, Quaid-e-Azam Campus, Lahore 54590, Pakistan*

[d] *Haihe Laboratory of Sustainable Chemical Transformations, Tianjin, 300192, China*

Received 3 September 2023; revised 20 November 2023; accepted 3 December 2023
Available online ■ ■ ■

Abstract

Charge separation is critical for achieving efficient solar-to-hydrogen conversion, whereas piezoelectric-enhanced photoelectrochemical (PEC) systems can effectively modulate band bending and charge migration. Herein, we design an n-TiO_2/$BaTiO_3$/p-TiO_2 (TBTm) heterojunction in which the piezoelectric $BaTiO_3$ layer is sandwiched between n-TiO_2 and p-TiO_2. The built-in electric field of TBTm can provide a strong driving force to accelerate carrier separation and prolong carrier lifetime. Consequently, the TBT3 achieves a prominent photocurrent density, as high as 2.13 mA•cm^{-2} at 1.23 V versus reversible hydrogen electrode (RHE), which is 2.4- and 1.5-times higher than TiO_2 and TiO_2–$BaTiO_3$ heterojunction, respectively. Driven by mechanical deformation, the induced dipole polarization can further regulate built-in electric fields, and the piezoelectric photocurrent density of TBT3-800 is 2.84 times higher than TiO_2 at 1.23 V *vs.* RHE due to the construction of piezoelectric-heterostructures. This work provides a piezoelectric polarization strategy for modulating the built-in electric field of heterojunction for PEC system.

Keywords: Photoelectrochemical; Piezoelectric polarization; Heterojunction; Charge separation

1. Introduction

The effective charge spatial separation is crucial for improving the solar-to-chemical conversion efficiency of photoelectrocatalysis [1,2]. In general, the charge transfer and migration paths is random in a single semiconductor, and severe recombination will occur between photogenerated electrons and holes, then reducing photoelectrochemical (PEC) efficiency. Engineering heterojunction has been proven to be one of the most promising methods for the construction of advanced PEC systems because of their feasibility and effectiveness for spatial charge separation [3–7]. The hybridization of semiconductors with diverse band structures leads to charge redistribution at the contact interface, and a built-in electric field *via* band bending will form in the space charge region for facilitating carrier separation [8,9].

Compared with typical type-II junction, the p-n junction can establish a very strong built-in electric field from n-type semiconductor to p-type semiconductor due to diffusion movements of majority carriers [10–14]. Several p-n heterojunctions, including p-Co_3O_4/n-Fe_2O_3 [15], p-Bi_2O_3/n-TiO_2

* Corresponding author. Key Laboratory for Green Chemical Technology of the Ministry of Education, School of Chemical Engineering and Technology, Tianjin University, Tianjin 300072, China.
E-mail address: panlun76@tju.edu.cn (L. Pan).

https://doi.org/10.1016/j.gee.2023.12.001

[16], n-TiO_2/p-Cu_2O [17], have been exploited for enhancing PEC performance. But the difficulty in energy band matching, interfacial and structural compatibility between different semiconductors is a challenge for desirable improvement of performances. Fortunately, p-n homojunction have been successfully established by finely controlling dopant or defect in semiconductors, by which the intrinsic conductivity could be modulated for homojunction construction [18,19]. Theoretically, oxygen vacancies of oxides as shallow donors possess n-type semiconducting property, while the cation vacancies show p-type conductivity and work as acceptor sites [20–22]. Hence, the TiO_2 p-n homojunction as the paradigm can be elaborately designed through the introduction of oxygen and titanium vacancies to achieve more efficiency in charge separation and transfer for significantly high photoactivity [23]. Importantly, p-n homojunction possesses the advantages of strong interaction, good component compatibility, and feasibility, which tend to form a successive band bending for promoting carrier separation and transfer [23–25]. However, the carrier separation efficiency of p-n junction may remain limited due to neutralizing the interfacial electric field through rapid accumulation of carriers during transfer process.

Piezoelectric effect with unique band tuning ability is arising as a revolutionary strategy to overcome the charge separation and transfer limitation of p-n heterojunction [26–28]. The permanent polarizations can be induced by piezoelectric materials with non-centrosymmetric structures, such as $BaTiO_3$ [29–31], $BiFeO_3$ [32,33] and $PbTiO_3$ [34,35] and can further be regulated by applying mechanical force. So, the advantage of the piezoelectric-heterostructures is that the width and magnitude of the space charge region at the contact interface can be easily altered with the piezoelectric polarization to regulate the charge migration [28]. However, the band alignment in piezoelectric-heterojunction should be elaborately designed to maximize charge separation enhancement.

Herein, we designed an n-TiO_2/$BaTiO_3$/p-TiO_2 heterojunction to couple with piezoelectric effect and p-n junctions. The piezoelectric $BaTiO_3$ is inserted between n-type TiO_2 and p-type TiO_2. Based on comprehensive characterizations of charge carrier behaviors in multi-heterojunction, the built-in electric field and polarized-induced electric field formed in heterojunction can provide a very strong driving force to enhance photo-carrier separation and prolong carrier lifetime. Therefore, the TBTm heterojunction shows excellent piezoelectric-enhanced PEC performance.

2. Experimental

2.1. Materials

Tetrabutyl titanate ($C_{16}H_{36}O_4Ti$) was purchased from Tianjin Guangfu Fine Chemical Research Institute. Diethylene glycol (DEG) was obtained from Tianjin HEOWNS Biochem Technologies. Isopropyl alcohol (IPA) was obtained from Tianjin Jiangtian Chemical Technology Co., LTD. Tetrabutylammonium hydroxide (TBAH, 40 wt% in H_2O) was obtained from J&K Scientific LLC. Hydrochloric acid (HCl), glycerol ($C_3H_8O_3$), barium hydroxide octahydrate ($Ba(OH)_2 \cdot 8H_2O$) and andethyl alcohol (C_2H_6O) were supplied by Tianjin Yuanli Chemical Industry Co., LTD.

2.2. Preparation of n-TiO_2/$BaTiO_3$/p-TiO_2 heterojunction

TiO_2 photoanodes was synthesized *via* a hydrothermal method. Typically, 0.17 mL of $C_{16}H_{36}O_4Ti$ were dissolved in a mixture of 8 mL HCl (36%–38 % by mass) and 12 mL H_2O. The FTO substrates were immersed and then heated in a steel-lined Teflon autoclave at 170 °C for 5 h. Then, the dry sample was annealed at 500 °C for 1 h in air to obtain TiO_2 photoanodes.

Then, 0.75 mmol $Ba(OH)_2 \cdot 8H_2O$ was dissolved in 7 mL H_2O, then 5 mL DEG, 5 mL ethanol, 1.5 mL IPA and 0.6 g TBAH were added successively, and stirred thoroughly. Then, the resulting solution and TiO_2 photoanode were transferred to a 50 mL Teflon autoclave and heated at 150 °C for 5 h. After cooling, the obtained TiO_2–$BaTiO_3$ heterojunction (named as TB) was washed and dried at 60 °C. The complete *in-situ* conversion can be achieved to obtain pure $BaTiO_3$ with the same process when increased $Ba(OH)_2 \cdot 8H_2O$ of 2.5 mmol. The XRD pattern is provided in Fig. S1 (Supplementary Information, SI).

Finally, titanium defect TiO_2 (p-TiO_2) was synthesized and supported on the surface by a general solvothermal-calcination method proposed by our group [21,36–38]. In a typical process, the synthesized TB was immersed in the mixture of glycerol (1 mL) and ethanol (19 mL) containing a certain amount of $C_{16}H_{36}O_4Ti$, and the solvothermal reaction was performed at 180 °C for 8 h. After washing and drying, samples were calcined at 400 °C for 1 h in air to obtain the final n-TiO_2/$BaTiO_3$/p-TiO_2 samples, which were named TBTm according to the amount of $C_{16}H_{36}O_4Ti$ (m = 1, 3 or 5 μL) added.

2.3. Photoelectrochemical (PEC) test

The PEC properties of TiO_2, TB and TBTm were performed with an electrochemical workstation (CHI 660E) with a typically three-electrode system with as-prepared samples, Pt electrode and Ag/AgCl as working, counter and reference electrode, respectively. The electrolyte was 1 M KOH aqueous (pH = 13.6). The light source was a 300 W Xenon lamp with an AM 1.5 G filter (100 mW/cm^2, PLS-SXE300UV, Beijing Perfectlight Technology. Co. Ltd.). Linear sweep voltammogram (LSV) were performed at the scanning speed of 10 mV/s. The electrochemical impedance spectroscopy (EIS) was analyzed with the sinusoidal AC voltage of 10 mV in the frequency range of 0.1–10^5 Hz under light conditions. The Nernst aquation was carried out to convert the measured potential of Ag/AgCl reference potential to reversible hydrogen electrode (RHE) scale: E (*vs.* RHE) = E (*vs.* Ag/AgCl) + 0.059 × pH + 0.197.

Please cite this article as: M. Ai et al., Piezoelectric-enhanced n-TiO_2/$BaTiO_3$/p-TiO_2 heterojunction for highly efficient photoelectrocatalysis, Green Energy & Environment, https://doi.org/10.1016/j.gee.2023.12.001

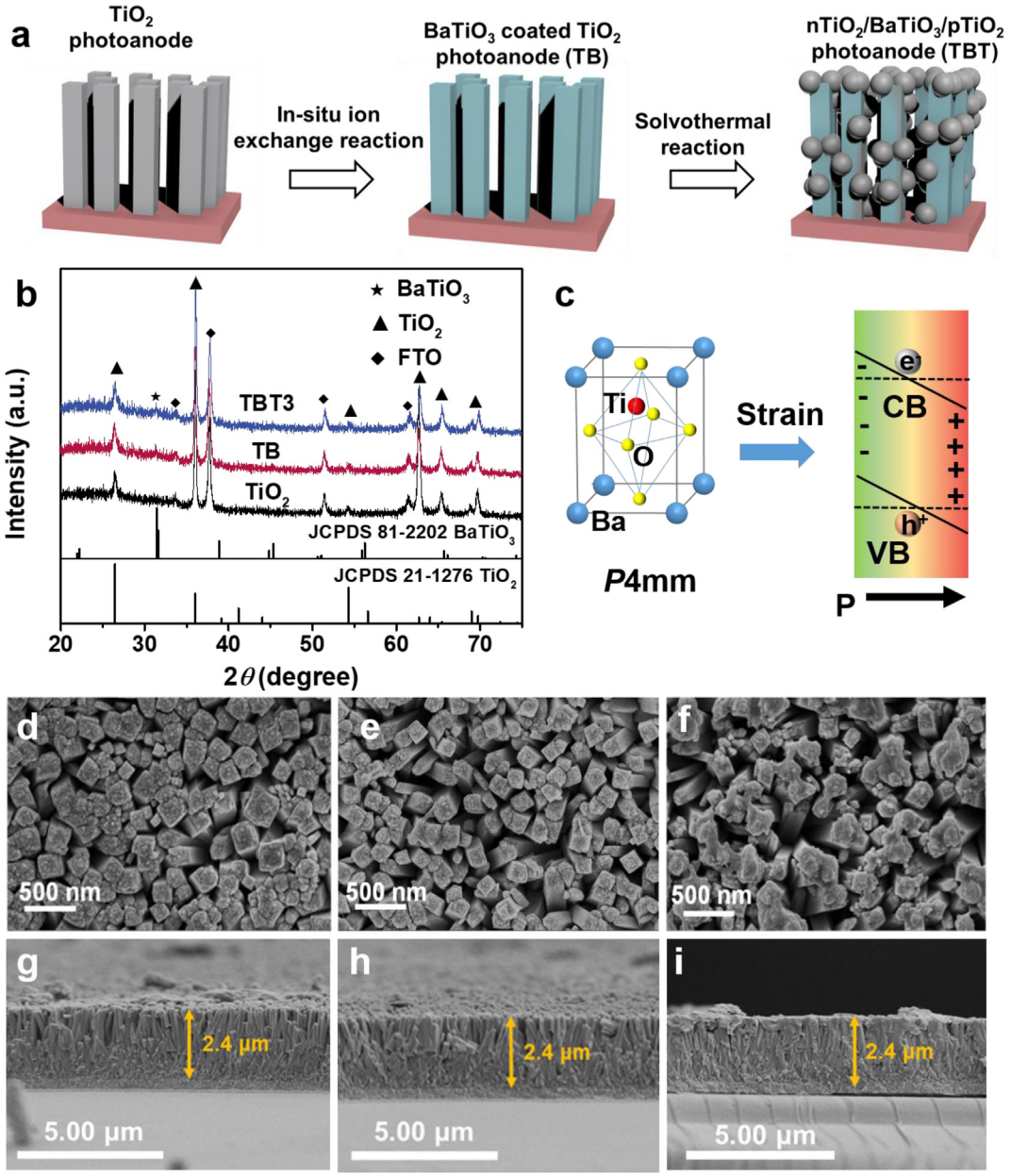

Fig. 1. (a) The fabrication process of n-TiO_2/$BaTiO_3$/p-TiO_2 heterojunction. (b) XRD patterns of TiO_2, TB and TBT3. (c) The crystal structure of tetragonal $BaTiO_3$ and schematic illustration of the piezotronic effect under strains. Top-view and cross-sectional SEM images of (d, g) TiO_2, (e, h) TB and (f, i) TBT3.

3. Results and discussion

3.1. Structural analysis of n-TiO_2/$BaTiO_3$/p-TiO_2 heterojunction

The n-TiO_2/$BaTiO_3$/p-TiO_2 (TBTm) heterojunction was synthesized *via* a step-by-step hydrothermal process (Fig. 1a). As shown in XRD patterns (Fig. 1b), TiO_2 nanorods (NRs) show characteristic peaks at 27.45°, 36.09° and 62.74°, corresponding to crystal planes of (110), (101) and (002) of rutile TiO_2 (JCPDS No. 21-1276) [39]. For TB and TBT3, an additional diffraction peak appears at 31.47°, which corresponds to (101) crystal plane of tetragonal $BaTiO_3$ (JCPDS No. 81-2202) with ferroelectric properties [40,41]. The relatively weak reflection signals of $BaTiO_3$ are attributed to the low content and the masking effect originated from high intensity reflection signals of TiO_2. $BaTiO_3$ has non-centrosymmetric crystal structure with a spontaneous polarization and can be regulated by an external mechanical force in Fig. 1c [42]. The formed polarized dipoles can enhance the spatial separation and directional transfer of photoexcited charges.

Top-view and cross-sectional SEM images of TiO_2 NRs show that vertically aligned TiO_2 NRs uniformly cover the FTO substrate with a thickness of *ca.* 2.40 μm (Fig. 1d and g). The diameter of TiO_2 NRs is *ca.* 190 nm (inset in Fig. 2a). The high-resolution TEM in Fig. 2a verifies the interplanar spacing of TiO_2 NRs is 0.32 nm, assigned to (110) plane of rutile TiO_2.

Please cite this article as: M. Ai et al., Piezoelectric-enhanced n-TiO_2/$BaTiO_3$/p-TiO_2 heterojunction for highly efficient photoelectrocatalysis, Green Energy & Environment, https://doi.org/10.1016/j.gee.2023.12.001

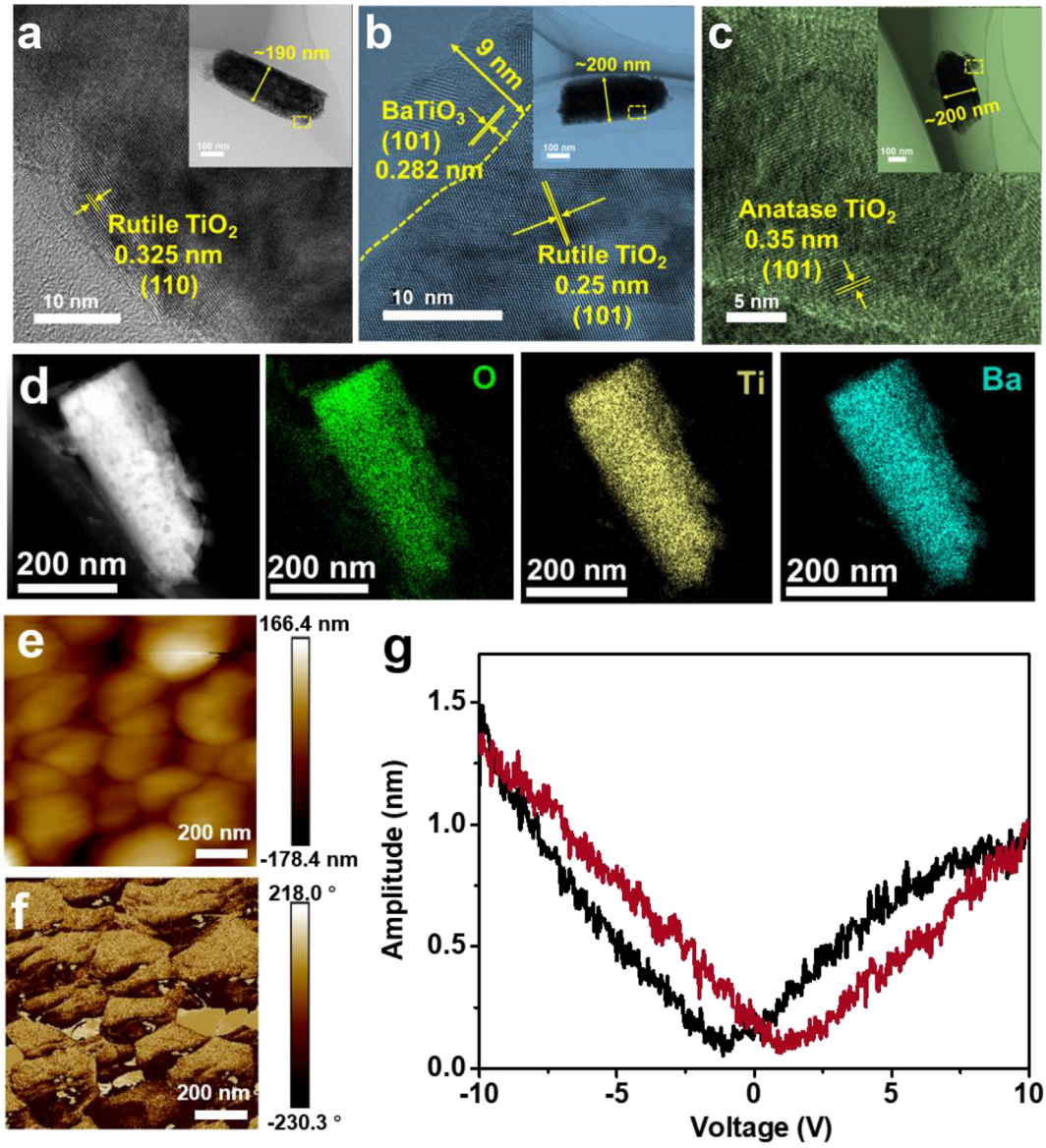

Fig. 2. TEM and HRTEM images of (a) TiO_2, (b) TB and (c) TBT3. (d) EDS mapping images of TBT3. (e) PFM amplitude image, (f) phase image, (g) amplitude butterfly loop of TBT3.

After *in-situ* ion exchange reaction, $BaTiO_3$ layers are formed without obvious changes in morphology and film thickness (Fig. 1e and h). The diameter of TB NRs slightly increases to *ca.* 200 nm (inset in Fig. 2b), with $BaTiO_3$ layer of *ca.* 9 nm (the lattice fringe of *ca.* 0.28 nm refers to (101) plane of $BaTiO_3$, Fig. 2b).

From Fig. 1f and i, TBT3 heterojunction is constructed by modifying Ti-defected TiO_2 (p-TiO_2) particles through solvothermal reaction. The morphology structure of Ti-defected TiO_2 is an irregular structure of self-assembled small particles. At the same time, the aggregation degree of Ti-defected TiO_2 will gradually increase with the increase of the addition amount of $C_{16}H_{36}O_4Ti$ as shown in Fig. S2 (SI). The scattered p-TiO_2 particles show the lattice spacing of *ca.* 0.35 nm, which is assigned to (101) crystal facet of anatase TiO_2 (Fig. 2c) [43]. The energy dispersive X-ray spectrometer (EDS) mapping (Fig. 2d) confirms the uniform distribution of Ti, O and Ba in TBT3, confirming the formation of n-TiO_2/$BaTiO_3$/p-TiO_2 multi-heterojunction. The piezoelectric properties of TiO_2, TB and TBT3 were characterized by a piezoresponse force microscope (PFM). In Figs. S3a–c (SI), TiO_2 NRs show no amplitude signal and have no intrinsic piezoelectric properties. In comparison, TB and TBT3 both show the typical piezoelectric butterfly ring, originating from the piezoelectric effect of $BaTiO_3$ layers (Figure S3d-f, SI and Fig. 2e–g) [31]. Compared to TB, the TBT3 heterojunction has a slightly reduced piezoelectric response due to further modification of Ti-defected TiO_2 particles.

The electronic coupling and valence states of samples were analyzed by X-ray photoelectron spectroscopy (XPS). The survey XPS spectra of TB and TBT3 show the presence of Ti, O and Ba elements without any impurities (Figs. S4 and SI). In Ti 2p XPS spectra, two main peaks of Ti 2p for TiO_2 are corresponding to Ti $2p_{1/2}$ and Ti $2p_{3/2}$, respectively, indicating

Please cite this article as: M. Ai et al., Piezoelectric-enhanced n-TiO_2/$BaTiO_3$/p-TiO_2 heterojunction for highly efficient photoelectrocatalysis, Green Energy & Environment, https://doi.org/10.1016/j.gee.2023.12.001

the existence of Ti^{4+} (Fig. 3a). After *in-situ* ion-exchange to TB, the binding energy of Ti $2p_{3/2}$ slightly shifts to lower binding energy compared with TiO_2, suggesting the change of coordination environment due to Ba^{2+} embedding [29]. After decorating with p-TiO_2, the Ti $2p_{3/2}$ peak in TBT3 shifts towards higher binding energy compared with both that of TB and TiO_2 owing to Ti vacancies with lower electron cloud density [21]. In Fig. 3b, the Ba 3d-binding energies are located at 795.2 and 779.8 eV, belonging to Ba $3d_{3/2}$ and Ba $3d_{5/2}$ orbitals of Ba^{2+} in $BaTiO_3$, respectively [29]. Notably, there is no significant peak shift of Ba 3d-binding energies between TB and TBT3 but there are significant changes in surface oxygen states among samples. The reason should be that the electron transfer between $BaTiO_3$ and TiO_2 is more through the Ti–O bond [44]. In Fig. 3c–e, the O 1s peak can be deconvolved into three peaks: lattice oxygen (O_L, 529.7 eV), oxygen vacancies (O_V, 531.4 eV), and adsorbed –OH/H_2O (O_{OH}, 532.8 eV) [45,46]. In Fig. 3f, TiO_2 exhibits intrinsic oxygen vacancies, and the peak area ratio of O_V/O_L is *ca.* 22 %. For TB heterojunction, the ratio of O_V/O_L increases to *ca.* 38 % due to the difference in lattice parameters between TiO_2 and $BaTiO_3$, which lead to form more oxygen vacancies through *in-situ* ion-exchange reaction. Significantly, the O_V/O_L ratio of TBT3 multi-heterojunction decreases to *ca.* 15 %, which is attributed to the introduction of Ti vacancies in the outer p-TiO_2 [23]. Electron paramagnetic resonance (EPR) measurements were carried out to further detect the changes of oxygen vacancies. TiO_2, TB and TBT3 possess obvious

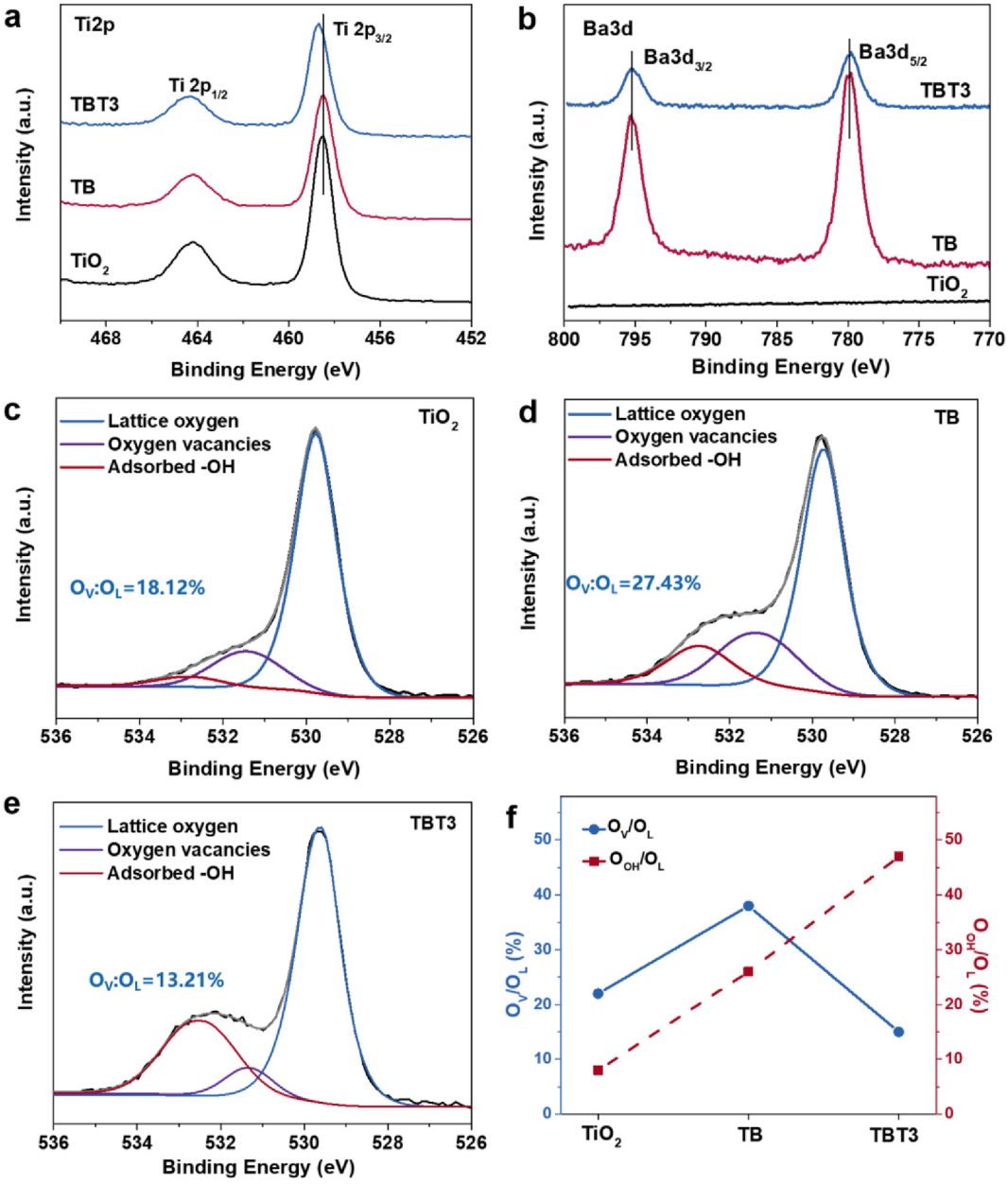

Fig. 3. (a) Ti 2p and (b) Ba 3d XPS spectra of TiO_2, TB and TBT3. O 1s XPS spectra of (c) TiO_2, (d) TB and (e) TBT3. (f) The peak area ratio of O_V/O_L and O_{OH}/O_L in TiO_2, TB and TBT3.

Please cite this article as: M. Ai et al., Piezoelectric-enhanced n-TiO_2/$BaTiO_3$/p-TiO_2 heterojunction for highly efficient photoelectrocatalysis, Green Energy & Environment, https://doi.org/10.1016/j.gee.2023.12.001

signals peak at 2.003, assigned to oxygen vacancies in Fig. S5 (SI) [47]. And the change trend of EPR signal is consistent with XPS results. For adsorbed −OH/H_2O on the surface, compared with TiO_2, the O_{OH}/O_L ratio of TB and TBT3 increases from 8 % to 26 % and 47 %, respectively. Ti vacancies in TBT3 can effectively enhance −OH/H_2O adsorption and energetically favorable H_2O oxidation with relatively low energy barrier [48].

3.2. Photoelectrochemical (PEC) performance

The PEC performance of all photoanodes was measured under AM 1.5G irradiation in a 1.0 M KOH electrolyte. As shown in Fig. 4a, TiO_2 exhibits a relatively lower photocurrent density of 0.88 mA•cm^{-2} at 1.23 V *vs.* RHE, and a high onset potential of 0.26 V *vs.* RHE. After *in-situ* growth of $BaTiO_3$, the photocurrent density of TB increases to 1.43 mA•cm^{-2} at 1.23 V *vs.* RHE. The various amount of p-TiO_2 is optimized in TBTm, with the order of TBT3 >TBT1 >TBT5. TBT3 performs optimal photocurrent density of 2.13 mA•cm^{-2} at 1.23 V *vs.* RHE, which is 2.4- and 1.5-times of the TiO_2 and TB, respectively. Meanwhile, the onset potential also decreases to 0.20 V *vs.* RHE. However, once excessive p-TiO_2 is decorated (TBT5), there is a serious agglomeration of nanoparticles which is detrimental to light absorption and photogenerated carrier separation and transfer, resulting in the reduction of photoelectrochemical activity.

The applied bias photon-to-current conversion efficiency (ABPE) of TBT3 shows the highest value of 0.49 % at 0.83 V *vs.* RHE, while TiO_2 and TB only reach the maximum value of 0.15 % at 0.96 V *vs.* RHE and 0.34 % at 0.86 V *vs.* RHE (Fig. 4b). Then, the incident photo-to-current conversion efficiency (IPCE) spectra were performed (Fig. 4c), ranked as TBT3 > TBT1 > TBT5 > TB > TiO_2. TBT3 sample reaches the maximum value of 90.84 % at 330 nm, which was 1.68 times higher than that of TiO_2 (54.22 %). Meanwhile, the PEC

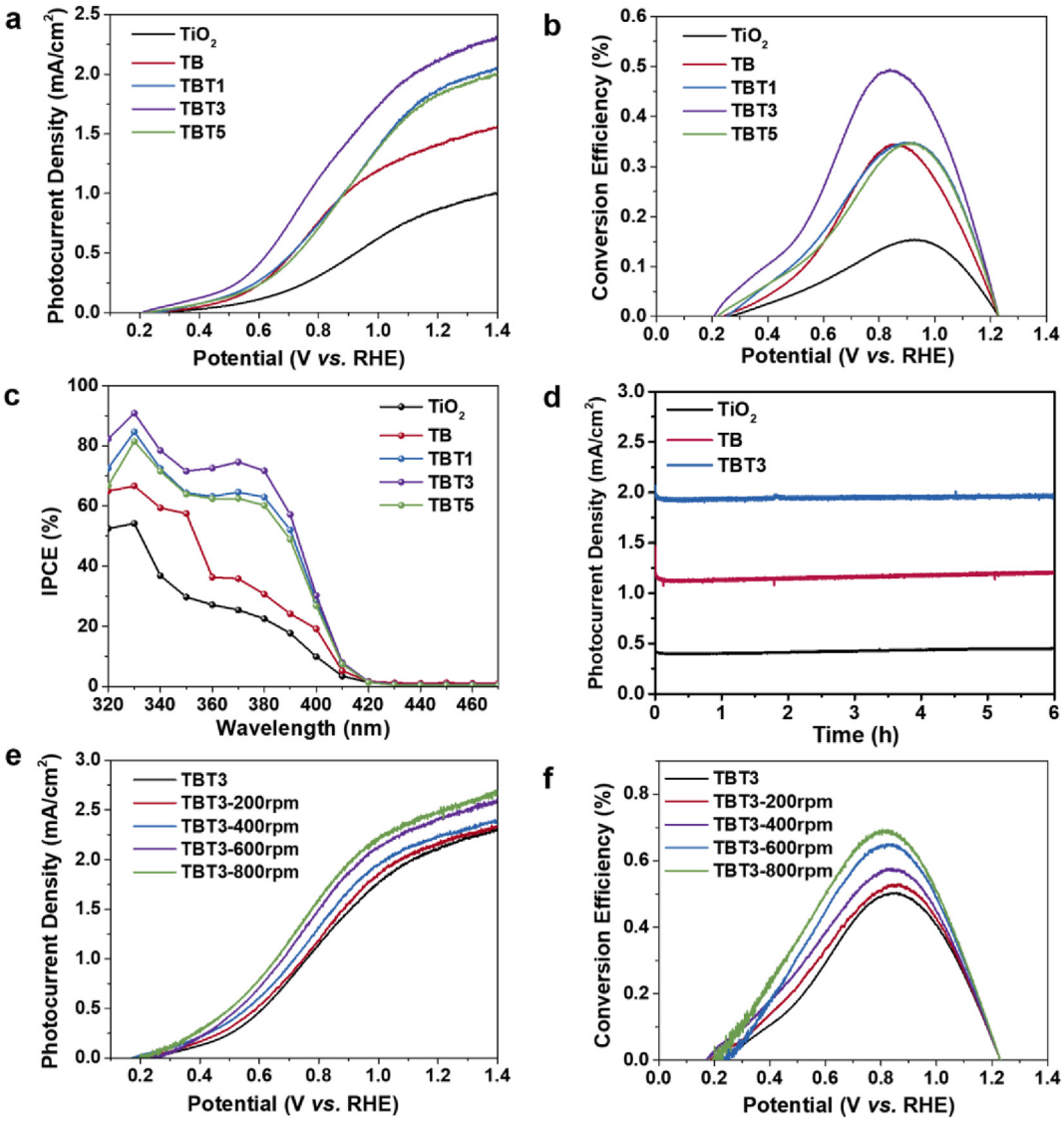

Fig. 4. (a) LSV, (b) ABPE curves, (c) IPCE of TiO_2, TB and TBTm. (d) Time-dependent photocurrent density of TiO_2, TB and TBT3 at 1.1 V *vs.* RHE. (e) LSV curves and (f) ABPE curves of TBT3 under different stirring speeds.

Please cite this article as: M. Ai et al., Piezoelectric-enhanced n-TiO_2/$BaTiO_3$/p-TiO_2 heterojunction for highly efficient photoelectrocatalysis, Green Energy & Environment, https://doi.org/10.1016/j.gee.2023.12.001

stability of TiO_2, TB and TBT3 was determined under continuous illumination for 6 h. As shown in Fig. 4d, all samples exhibit excellent stability.

Subsequently, the piezo-photoelectric performances of TiO_2, TB and TBT3 were measured by stirring-induced mechanical forces. The deformation of $BaTiO_3$ can generate an enhanced polarization electric field for TB and TBT3. The degree of piezoelectric effect is controlled by a stirring speed of 0−800 rpm and labeled as TiO_2-M, TB-M and TBT3-M (M represents stirring speed). In Fig. S6a and b (SI), TiO_2 NRs were tested under stirring at different speeds in the dark and under irradiation. The piezo-photocurrent density of TiO_2 NRs both have almost no change with the increase of stirring speed, suggesting no piezoelectric enhancement or mass transfer enhancement. In comparison, TB and TBT3 show the piezoelectric current of with increased stirring speed in the dark due to the piezoelectric effect (Fig. S6c,e, SI). It is worth noting that the piezoelectric current is only two orders of magnitude smaller than the piezo-photocurrent density so that the contribution to the piezoelectric current is negligible. Under irradiation, the piezo-photocatalytic activity of TB shows 1.11-times enhancement at 1.23 V *vs.* RHE under a stirring speed 800 rpm (Fig. S6d and SI). In Fig. 4e, the piezo-photocatalytic activity of TBT3 increases gradually with the increase of stirring rate. When the stirring rate is 800 rpm, the photocurrent density of TBT3-800 increases to 2.50 $mA \cdot cm^{-2}$ at 1.23 V *vs.* RHE with an enhancement of 2.84 times compared with TiO_2 without stirring. It is worth noting that the performance of TBT3-800 is better than most representative TiO_2-based photoanodes reported previously (Table S1 and SI). The corresponding ABPE of TBT3-800 reaches a maximum value of 0.69 % at 0.8 V *vs.* RHE (Fig. 4f). The enhanced piezo-photocatalytic performance may be attributed to the strong driving force of deformation-enhanced charge separation.

3.3. Charge carrier behaviors in heterojunction

The charge carrier behaviors in n-TiO_2/$BaTiO_3$/p-TiO_2 heterojunction were then evaluated. The efficient charge separation of TBT3 multi-heterojunction was proved by photoluminescence (PL) spectra in Fig. 5a. The lower PL intensity of TBT3 than pristine TiO_2 and TB indicates that TBT3 has lower carrier recombination rate, which favors high charge-separation efficiency. According to the fitted time-resolved PL curves, the average carrier lifetime of TiO_2, BT and TBT3 are 1.88, 2.49 and 3.28 ns, respectively (Fig. 5b and Table S2 and SI). The prolonged carrier lifetime in TBT3 leads to reduced radiative recombination of photogenerated carriers [49].

Subsequently, the charge injection and charge separation efficiencies were evaluated by using Na_2SO_3 as hole scavengers in PEC water oxidation system (1 M KOH) [50,51] in Fig. S7a–c (SI). As shown in Fig. S7d (SI), surface charge injection efficiency (η_{inj}) values are 62.3 %, 64.4 %, and 64.1 % for TiO_2, TB and TBT3 (at 1.23 V *vs.* RHE), respectively, indicating η_{inj} is not the pivotal reason for the enhancement of PEC photoactivity [52]. Noticeably, the charge separation efficiency (η_{sep}) of TiO_2, TB and TBT3 are calculated as 43.6 %, 60.6 % and 86.6 % at 1.23 V *vs.* RHE (Fig. 5c). The η_{sep} values of TB and TBT3 are enhanced by *ca.* 139 % and 199 % compared with TiO_2, which is consistent with the increased PEC photocurrent density. The above results confirm that TBT3 heterostructure can efficiently enhance carrier separation and suppress electron–hole recombination owing to the formation of the internal electric field and polarized-induced electric field.

Open circuit photo-voltage (OCP) measurements were conducted to verify the intensity of built-in electric field in heterojunction (Fig. 5d). Photovoltage ($\Delta OCP = OCP_{dark} - OCP_{light}$) derived from the open-circuit voltage in dark (OCP_{dark}) and under light (OCP_{light}) follows the order: TBT3 (0.89 V) > TB (0.80 V) > TiO_2 (0.74 V). Such a large ΔOCP indicates a strong intrinsic built-in electric field, which enhances the driving force of charge separation. Besides, the OCP transient decay measurement (Fig. S8 and SI) was used to evaluate the lifetime of photogenerated carriers. The strong band bending can create a large number of spatial charges in the depletion layer so that remarkable carrier recombination occurs immediately in the transient once illumination is turned off [53,54]. Thus, compared with TiO_2 (178 ms) and TB (128 ms), the fast decay kinetic constant of 72 ms further confirms effective charge separation due to the stronger band bending and built-in electric field in TBT3 [53,54]. Besides, the significant decrease in the onset potential of TBT3 is also attributed to the larger ΔOCP provided by the stronger built-in electric field.

To evaluate charge transfer behaviors at the interface of photoanode/electrolyte, electrochemical impedance spectroscopy (EIS) was monitored at open-circuit potential. As demonstrated in Fig. 5e, the Nyquist plots of TiO_2 shows a large semicircle, and the fitted charge transfer resistance at the interface is *ca.* 1816 Ω. BT with $BaTiO_3$ deposition exhibits a smaller semicircle compared with TiO_2 and a lower charge-transfer resistance of *ca.* 1139 Ω. Obviously, TBT3 with n-TiO_2/$BaTiO_3$/p-TiO_2 structure shows two obvious semicircles. The small semicircle in the high-frequency range is usually regarded as a charge bulk transfer process of photoanode and the large semicircle of low-frequency region is related to charge transfer behavior at the Helmholtz layer [55]. As the equivalent circuit model fitted (inserted in Fig. 5f), the values of R_{bulk} (121.3 Ω) and R_{ct} (346 Ω) for TBT3 obviously decrease, demonstrating an improved charge transfer in the bulk and interface. Meanwhile, a significant decrease was observed in R_{bulk} by applying the external mechanical forces on TBT3 in Fig. 5f [56]. Internal electric field and polarized-induced electric field formed in n-TiO_2/$BaTiO_3$/p-TiO_2 heterojunction can provide an effective driving force to enhance photo-carrier separation.

3.4. Photoelectrocatalytic mechanism of heterojunction

To further explore the enhancement mechanism of PEC performance, the band structure and charge transfer pathway of TBT3 were investigated. From Fig. 6a and b (UV-vis DRS spectra), TiO_2 and $BaTiO_3$ exhibit the band gap of 3.07 and

Please cite this article as: M. Ai et al., Piezoelectric-enhanced n-TiO_2/$BaTiO_3$/p-TiO_2 heterojunction for highly efficient photoelectrocatalysis, Green Energy & Environment, https://doi.org/10.1016/j.gee.2023.12.001

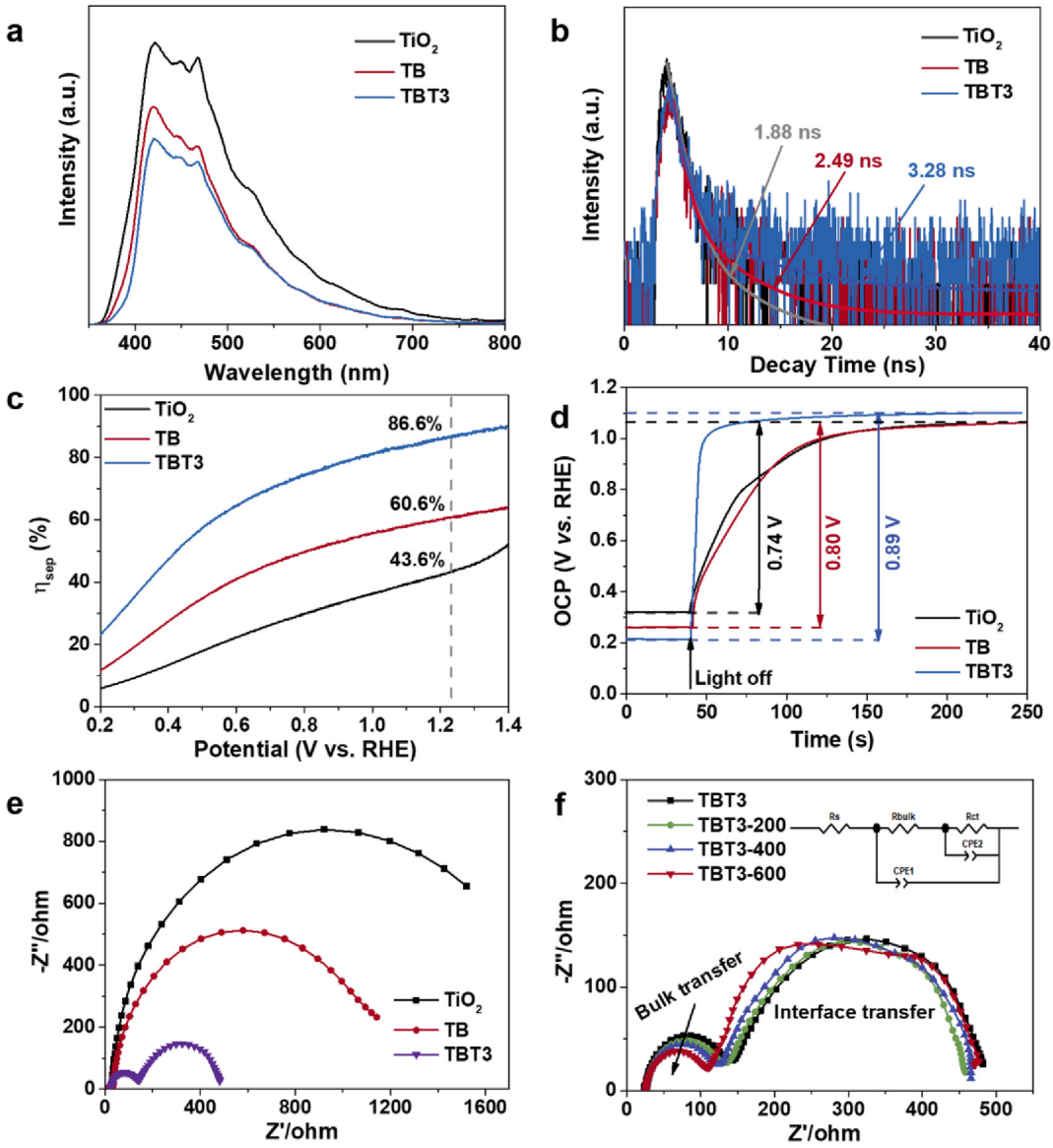

Fig. 5. (a) PL spectra and (b) TRPL spectra of TiO_2, TB and TBT3. (c) The charge separation efficiency and (d) OCP measurements of TiO_2, TB, and TBT3. (e) EIS Nyquist plots of TiO_2, TB and TBT3. (f) EIS Nyquist plots of TiO_2, TB and TBT3 under different stirring speeds. Inset: equivalent circuit used for fitting EIS spectra.

3.09 eV, respectively. TB and TBT3 show the similar band edge but the latter has the enhanced UV absorption. Furthermore, Mott–Schottky (M–S) curves show that TiO_2, $BaTiO_3$ and TB show positive M–S curves and endow with n-type conductivity (Fig. 6c). And TiO_2 and $BaTiO_3$ have flat-band potentials of 0.12 eV and −0.11 eV *vs.* RHE, respectively. The position of E_f potential of n-type semiconductor is 0.1–0.3 eV lower than that of CB potential as previous reported [57,58]. Therefore, the CB of TiO_2 and $BaTiO_3$ is determined as *ca.* −0.08 and −0.31 eV, respectively. Thus, the band structures of TiO_2 and $BaTiO_3$ can be derived and shown in Fig. S9 (SI). According to band alignment, a type II heterojunction tends to form between TiO_2 and $BaTiO_3$ in TB [29]. Differently, the M–S plot of TBT3 shows a typical inverted "V-shaped" (Fig. 6d), indicating the typical characteristic of p-n junction due to the introduction of p-TiO_2 [59,60]. The positive M–S part of the flat band potential of *ca.* 0.12 V *vs.* RHE is mainly contributed by the hybrid of n-type TiO_2 and $BaTiO_3$, while the negative M–S plots originates from V_{Ti}–TiO_2 (featuring p-type conductivity) [61,62].

Thus, the enhanced charge separation mechanism of TBT3 is proposed. First, TiO_2 tends to form oxygen vacancies as shallow donors and features n-type conductivity. Whereas V_{Ti} can capture electrons and contribute to p-type conductivity, which results in the Fermi level close to the valence band [20,23]. As a result, the introduction of metal defects increases the Fermi energy level difference between rutile n-TiO_2 and anatase p-TiO_2, forming an n-p homojunction, and an enhanced built-in electric field can be formed [23], whose performance is much higher than that of n-TiO_2/n-TiO_2 homojunction (Figs. S10 and SI). In particular, $BaTiO_3$ plays the crucial role in enhancing charge separation in TBT3. On one hand, $BaTiO_3$ is a typical

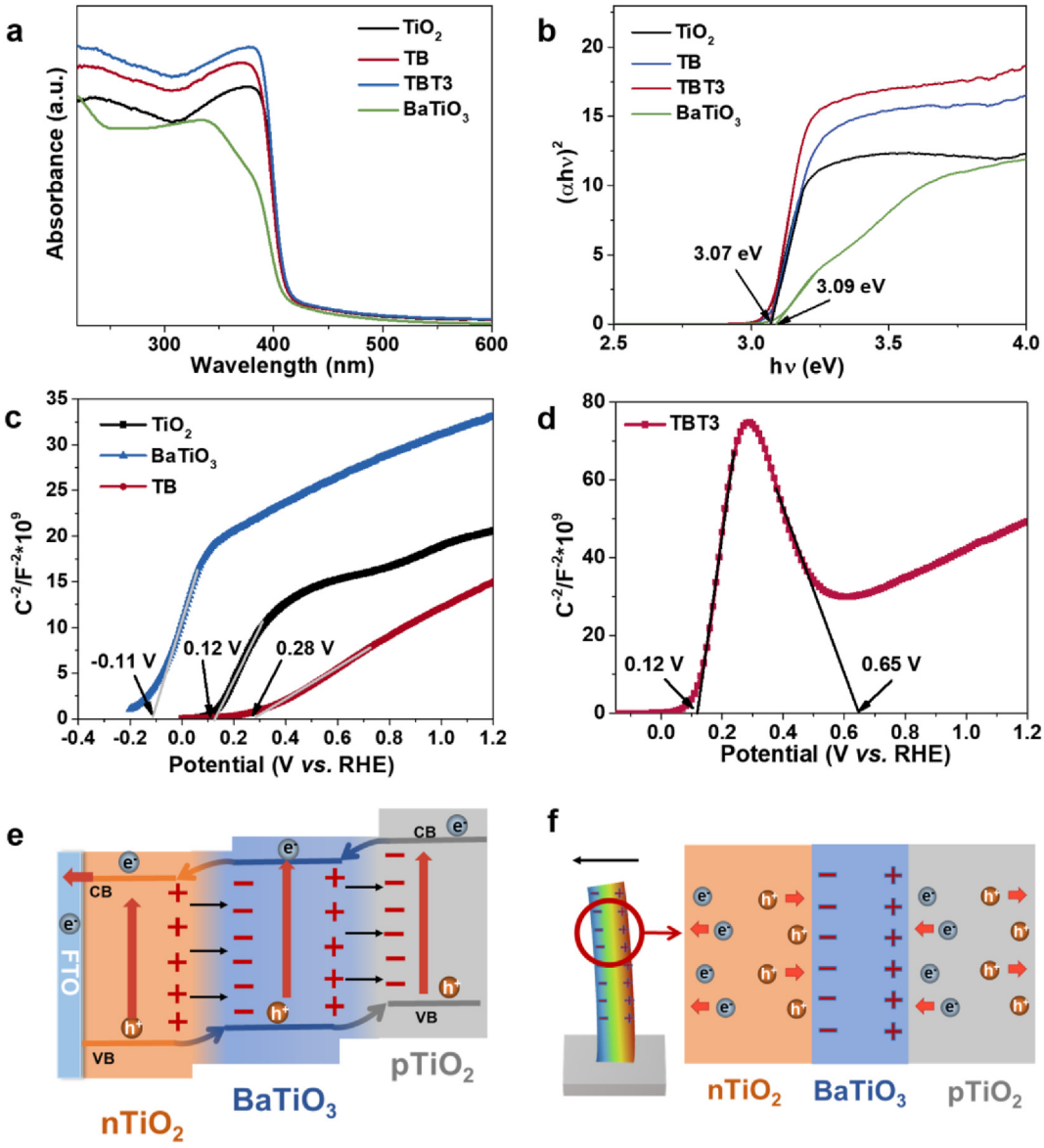

Fig. 6. (a) UV-vis DRS and (b) Kubelka–Munk energy curve plots of TiO_2, TB, TBT3 and $BaTiO_3$. (c, d) M−S curves of TiO_2, $BaTiO_3$, TB and TBT3. (e) Electron transfer process for n-TiO_2/$BaTiO_3$/p-TiO_2 under illumination. (f) Mechanism for the piezoelectric-enhanced PEC performance under both illumination and stirring.

piezoelectric material that can be spontaneously polarized by the displacements of symmetric centers of negative and positive charges in a crystal unit cell [26]. When $BaTiO_3$ is inserted into n-TiO_2 and p-TiO_2, the spontaneous polarization of built-in electric field is conducive to enhancing the tandem II type electron transfer pathway in TBT3 (Fig. 6e). Under photoexcitation, the electrons in TBT3 were smoothly transmitted to the inner rutile n-TiO_2, and p-TiO_2 works as hole-collecting layers for driving H_2O oxidation. On the other hand, the spontaneous polarization in $BaTiO_3$ can be aligned by mechanical deformation, which can effectively promote the charges separation of p-n heterojunction.

As illustrated in Fig. 6f, the piezoelectric-induced negative charges of $BaTiO_3$ layer will attract photogenerated holes in n-TiO_2. And the positive charge induced by piezoelectricity will attract the photogenerated electrons in p-TiO_2. As a result, the piezoelectric effect triggered by mechanical energy greatly promotes carrier separation process to prolong the carrier lifetime and significantly improve photoelectrocatalytic performance.

4. Conclusion

In this work, we designed an n-TiO_2/$BaTiO_3$/p-TiO_2 heterojunction in which the ferroelectric $BaTiO_3$ layer is between n-TiO_2 with oxygen vacancies and p-TiO_2 with titanium vacancies. Such multi-heterojunction with well-aligned band structure can form a built-in electric field and polarized-induced electric field at the interface to promote carrier separation and extend carrier lifetime. Consequently, the outstanding PEC performance on TBT3 multi-heterostructures of 2.13 mA cm^{-2} (at 1.23 V *vs.* RHE) is achieved, which is *ca.* 2.4-times and 1.5-

Please cite this article as: M. Ai et al., Piezoelectric-enhanced n-TiO_2/$BaTiO_3$/p-TiO_2 heterojunction for highly efficient photoelectrocatalysis, Green Energy & Environment, https://doi.org/10.1016/j.gee.2023.12.001

times higher than TiO_2 and TB. Meanwhile, because the ferroelectric $BaTiO_3$ form a stable polarized electric field by mechanical deformation, the current density is up to 2.50 mA/cm^2 at 1.23 V *vs.* RHE. This work provides new insights into an enhanced built-in electric field in multi-heterojunction through synergistic piezoelectric effects and vacancy engineering.

CRediT authorship contribution statement

Minhua Ai: Conceptualization, Data curation, Formal analysis, Investigation, Writing − original draft, Writing − review & editing, Visualization. **Zihang Peng:** Data curation, Formal analysis, Validation, Writing − original draft, Visualization. **Xidi Li:** Formal analysis, Software, Validation, Visualization. **Faryal Idrees:** Funding acquisition, Writing − review & editing. **Xiangwen Zhang:** Resources, Supervision. **Ji-Jun Zou:** Funding acquisition, Project administration, Supervision. **Lun Pan:** Conceptualization, Funding acquisition, Supervision, Writing − review & editing, Methodology, Project administration, Resources.

Conflict of interest

The authors declare that they have no known competing financial interests or personal relationships that could have appeared to influence the work reported in this paper.

Acknowledgement

The authors appreciate the support from the National Natural Science Foundation of China (22222808, 21978200, 22161142002), the Joint Research Programs of National Natural Science Foundation of China and Pakistan Science Foundation (PSF-NSFC-IV/Phy/P-PU(31)), and the Haihe Laboratory of Sustainable Chemical Transformations for financial support.

Appendix A. Supplementary data

Supplementary data to this article can be found online at https://doi.org/10.1016/j.gee.2023.12.001.

References

[1] Y. Zhang, Y. Bu, L. Wang, J.-P. Ao, Regulation of the photogenerated carrier transfer process during photoelectrochemical water splitting: A review, Green Energy Environ. 6 (2021) 479–495.
[2] S. Bai, J. Jiang, Q. Zhang, Y. Xiong, Steering charge kinetics in photocatalysis: intersection of materials syntheses, characterization techniques and theoretical simulations, Chem. Soc. Rev. 44 (2015) 2893–2939.
[3] F. Li, L. Cheng, J. Fan, Q. Xiang, Steering the behavior of photogenerated carriers in semiconductor photocatalysts: a new insight and perspective, J. Mater. Chem. A 9 (2021) 23765–23782.
[4] J. Huang, Y. Wang, K. Chen, T. Liu, Q. Wang, Boosting the photoelectrochemical water oxidation performance of bismuth vanadate by $ZnCo_2O_4$ nanoparticles, Chin. Chem. Lett. 33 (2022) 2060–2064.
[5] Z. Chi, J. Zhao, Y. Zhang, H. Yu, H. Yu, The fabrication of atomically thin-MoS_2 based photoanodes for photoelectrochemical energy conversion and environment remediation: A review, Green Energy Environ. 7 (2022) 372–393.
[6] L. Meng, L. Li, Recent research progress on operational stability of metal oxide/sulfide photoanodes in photoelectrochemical cells, Nano Res. Energy 1 (2022) e9120020.
[7] Y. Du, B. Li, G. Xu, L. Wang, Recent advances in interface engineering strategy for highly-efficient electrocatalytic water splitting, InfoMat 5 (2022) e12377.
[8] J. Li, L. Wang, W. Wang, X. Jia, Y. Zhang, H. Yang, Y. Li, Q. Zhou, Cooperative effects of surface plasmon resonance and type-II band alignment to significantly boost photoelectrochemical H_2 generation of TiO_2/CdS/TiN nanorod array photoanode, Appl. Catal., B 334 (2023) 122833.
[9] W. Zhai, Y. Ma, D. Chen, J.C. Ho, Z. Dai, Y. Qu, Recent progress on the long-term stability of hydrogen evolution reaction electrocatalysts, InfoMat 4 (2022) e12357.
[10] X. Tao, Y. Zhao, S. Wang, C. Li, R. Li, Recent advances and perspectives for solar-driven water splitting using particulate photocatalysts, Chem. Soc. Rev. 51 (2022) 3561−3608.
[11] H. Li, T. Wang, S. Liu, Z. Luo, L. Li, H. Wang, Z.J. Zhao, J. Gong, Controllable distribution of oxygen vacancies in grain boundaries of p-Si/TiO_2 heterojunction photocathodes for solar water splitting, Angew. Chem. Int. Ed. 60 (2021) 4034–4037.
[12] Y. Yang, W. Cheng, Y.F. Cheng, Preparation of Co_3O_4@ZnO core-shell nanocomposites with intrinsic p-n junction as high-performance photoelectrodes for photoelectrochemical cathodic protection under visible light, Appl. Surf. Sci. 476 (2019) 815–821.
[13] I. Vamvasakis, I.T. Papadas, T. Tzanoudakis, C. Drivas, S.A. Choulis, S. Kennou, G.S. Armatas, Visible-light photocatalytic H_2 production activity of β-$Ni(OH)_2$-modified CdS mesoporous nanoheterojunction networks, ACS Catal. 8 (2018) 8726–8738.
[14] H. Bai, X. Li, Y. Zhao, W. Fan, Y. Liu, Y. Gao, D. Xu, J. Ding, W. Shi, Fabrication of $BiVO_4$-Ni/Co_3O_4 photoanode for enhanced photoelectrochemical water splitting, Appl. Surf. Sci. 538 (2021) 148150.
[15] S.-S. Yi, B.-R. Wulan, J.-M. Yan, Q. Jiang, Highly efficient photoelectrochemical water splitting: Surface modification of cobalt-phosphate-loaded Co_3O_4/Fe_2O_3 p-n heterojunction nanorod arrays, Adv. Funct. Mater. 29 (2019) 1801902.
[16] L. Luo, W. Chen, S.M. Xu, J. Yang, M. Li, H. Zhou, M. Xu, M. Shao, X. Kong, Z. Li, H. Duan, Selective photoelectrocatalytic glycerol oxidation to dihydroxyacetone via enhanced middle hydroxyl adsorption over a Bi_2O_3-incorporated catalyst, J. Am. Chem. Soc. 144 (2022) 7720−7730.
[17] A. Rubino, R. Zanoni, P.G. Schiavi, A. Latini, F. Pagnanelli, Two-Dimensional restructuring of Cu_2O can Improve the performance of nanosized n-TiO_2/p-Cu_2O photoelectrodes under UV-Visible light, ACS Appl. Mater. Interfaces 13 (2021) 47932−47944.
[18] X.J. Guan, S.C. Zong, S.H. Shen, Homojunction photocatalysts for water splitting, Nano Res. 15 (2022) 10171−10184.
[19] Y. Ma, Y. Zhang, M. Xing, S. Kang, M. Du, B. Qiu, Y. Chai, Spin state engineering of spinel oxides by integration of Cr doping and a p-n junction for water oxidation, Chem. Commun. 58 (2022) 6642−6645.
[20] S. Wang, L. Pan, J.J. Song, W. Mi, J.J. Zou, L. Wang, X. Zhang, Titanium-defected undoped anatase TiO_2 with p-type conductivity, room-temperature ferromagnetism, and remarkable photocatalytic performance, J. Am. Chem. Soc. 137 (2015) 2975−2983.
[21] L. Pan, M. Ai, C. Huang, L. Yin, X. Liu, R. Zhang, S. Wang, Z. Jiang, X. Zhang, J.J. Zou, W. Mi, Manipulating spin polarization of titanium dioxide for efficient photocatalysis, Nat. Commun. 11 (2020) 418.
[22] L. Pan, S. Wang, W. Mi, J. Song, J.-J. Zou, L. Wang, X. Zhang, Undoped ZnO abundant with metal vacancies, Nano Energy 9 (2014) 71−79.
[23] L. Pan, S. Wang, J. Xie, L. Wang, X. Zhang, J.-J. Zou, Constructing TiO_2 p-n homojunction for photoelectrochemical and photocatalytic hydrogen generation, Nano Energy 28 (2016) 296−303.

[24] Z. Ai, Y. Shao, B. Chang, L. Zhang, J. Shen, Y. Wu, B. Huang, X. Hao, Rational modulation of p-n homojunction in P-doped g-C_3N_4 decorated with Ti_3C_2 for photocatalytic overall water splitting, Appl. Catal., B 259 (2019) 118077.
[25] G. Zhao, S. Hao, J. Guo, Y. Xing, L. Zhang, X. Xu, Design of p-n homojunctions in metal-free carbon nitride photocatalyst for overall water splitting, Chin. J. Catal. 42 (2021) 501−509.
[26] L. Pan, S. Sun, Y. Chen, P. Wang, J. Wang, X. Zhang, J.J. Zou, Z.L. Wang, Advances in piezo-phototronic effect enhanced photocatalysis and photoelectrocatalysis, Adv. Energy Mater. 10 (2020) 2000214.
[27] F. Chen, H. Huang, L. Guo, Y. Zhang, T. Ma, The role of polarization in photocatalysis, Angew. Chem. Int. Ed. 58 (2019) 10061−10073.
[28] Y. Yu, X. Wang, Piezotronics in photo-electrochemistry, Adv. Mater. 30 (2018) 1800154.
[29] Y. Liu, Z. Wang, C. Lin, J. Zhang, J. Feng, B. Hou, W. Yan, M. Li, Z. Ren, Spontaneous polarization of ferroelectric heterostructured nanorod arrays for high-performance photoelectrochemical cathodic protection, Appl. Surf. Sci. 609 (2023) 155345.
[30] C. Yu, J. He, M. Tan, Y. Hou, H. Zeng, C. Liu, H. Meng, Y. Su, L. Qiao, T. Lookman, Y. Bai, Selective enhancement of photo-piezocatalytic performance in $BaTiO_3$ via heterovalent ion doping, Adv. Funct. Mater. 32 (2022) 2209365.
[31] Q. Liu, F. Zhan, H. Luo, D. Zhai, Z. Xiao, Q. Sun, Q. Yi, Y. Yang, D. Zhang, Mechanism of interface engineering for ultrahigh piezo-photoelectric catalytic coupling effect of $BaTiO_3$@TiO_2 microflowers, Appl. Catal., B 318 (2022) 121817.
[32] M.L. Xu, M. Lu, G.Y. Qin, X.M. Wu, T. Yu, L.N. Zhang, K. Li, X. Cheng, Y.Q. Lan, Piezo-photocatalytic synergy in $BiFeO_3$ @COF Z-Scheme heterostructures for high-efficiency overall water splitting, Angew. Chem. Int. Ed. 61 (2022) 202210700.
[33] H. You, Z. Wu, L. Zhang, Y. Ying, Y. Liu, L. Fei, X. Chen, Y. Jia, Y. Wang, F. Wang, S. Ju, J. Qiao, C.H. Lam, H. Huang, Harvesting the vibration energy of $BiFeO_3$ nanosheets for hydrogen evolution, Angew. Chem. Int. Ed. 58 (2019) 11779−11784.
[34] G. Wan, L. Yin, X. Chen, X. Xu, J. Huang, C. Zhen, H. Zhu, B. Huang, W. Hu, Z. Ren, H. Tian, L. Wang, G. Liu, H.M. Cheng, Photocatalytic overall water splitting over $PbTiO_3$ modulated by oxygen vacancy and ferroelectric polarization, J. Am. Chem. Soc. 144 (2022) 20342−20350.
[35] Y. Liu, S. Ye, H. Xie, J. Zhu, Q. Shi, N. Ta, R. Chen, Y. Gao, H. An, W. Nie, H. Jing, F. Fan, C. Li, Internal-field-enhanced charge separation in a single-domain ferroelectric $PbTiO_3$ photocatalyst, Adv. Mater. 32 (2020) 1906513.
[36] Y. Li, T. Wang, M. Asim, L. Pan, R. Zhang, Z.-F. Huang, Z. Chen, C. Shi, X. Zhang, J.-J. Zou, Manipulating spin polarization of defected Co_3O_4 for highly efficient electrocatalysis, Trans. Tianjin Univ. 28 (2022) 163−173.
[37] R. Zhang, Y.-C. Zhang, L. Pan, G.-Q. Shen, N. Mahmood, Y.-H. Ma, Y. Shi, W. Jia, L. Wang, X. Zhang, W. Xu, J.-J. Zou, Engineering cobalt defects in cobalt oxide for highly efficient electrocatalytic oxygen evolution, ACS Catal. 8 (2018) 3803−3811.
[38] Y.-C. Zhang, S. Ullah, R. Zhang, L. Pan, X. Zhang, J.-J. Zou, Manipulating electronic delocalization of Mn_3O_4 by manganese defects for oxygen reduction reaction, Appl. Catal., B 277 (2020) 119247.
[39] R. Song, H. Chi, Q. Ma, D. Li, X. Wang, W. Gao, H. Wang, X. Wang, Z. Li, C. Li, Highly efficient degradation of persistent pollutants with 3D nanocone TiO_2-based photoelectrocatalysis, J. Am. Chem. Soc. 143 (2021) 13664−13674.
[40] C. Yang, Y. Chen, T. Chen, S. Rajendran, Z. Zeng, J. Qin, X. Zhang, A long-standing polarized electric field in TiO_2@$BaTiO_3$/CdS nanocomposite for effective photocatalytic hydrogen evolution, Fuel 314 (2022) 122758.
[41] X. Zhou, B. Shen, A. Lyubartsev, J. Zhai, N. Hedin, Semiconducting piezoelectric heterostructures for piezo- and piezophotocatalysis, Nano Energy 96 (2022) 107141.
[42] M. Acosta, N. Novak, V. Rojas, S. Patel, R. Vaish, J. Koruza, G.A. Rossetti, J. Rödel, $BaTiO_3$-based piezoelectrics: Fundamentals, current status, and perspectives, Appl. Phys. Rev. 4 (2017) 041305.
[43] F. Xu, K. Meng, B. Cheng, S. Wang, J. Xu, J. Yu, Unique S-scheme heterojunctions in self-assembled TiO_2/$CsPbBr_3$ hybrids for CO_2 photoreduction, Nat. Commun. 11 (2020) 4613.
[44] X. Zhou, X. Wang, T. Tan, H. Ma, H. Tang, X.a. Luo, F. Dong, Y. Yang, Unique S-scheme TiO_2/$BaTiO_3$ heterojunctions promote stable photocatalytic mineralization of toluene in air, Chem. Eng. J. 470 (2023) 143933.
[45] X. Pang, H. Bai, H. Zhao, W. Fan, W. Shi, Efficient Electrocatalytic Oxidation of 5-Hydroxymethylfurfural Coupled with 4-Nitrophenol Hydrogenation in a Water System, ACS Catal. 12 (2022) 1545−1557.
[46] X. Pang, H. Bai, Y. Huang, H. Zhao, G. Zheng, W. Fan, Mechanistic insights for dual-species evolution toward 5-hydroxymethylfurfural oxidation, J. Catal. 417 (2023) 22−34.
[47] S.M. Wu, Y.T. Wang, S.T. Xiao, L.Y. Wang, G. Tian, J.B. Chen, J.W. Liu, M. Shalom, X.Y. Yang, A spatial homojunction of titanium vacancies decorated with oxygen vacancies in TiO_2 and its directed charge transfer, Nanoscale 14 (2022) 13373−13377.
[48] T. Wang, L. Liu, G. Ge, M. Liu, W. Zhou, K. Chang, F. Yang, D. Wang, J. Ye, Two-dimensional titanium oxide nanosheets rich in titanium vacancies as an efficient cocatalyst for photocatalytic water oxidation, J. Catal. 367 (2018) 296−305.
[49] Y. Xiao, Z. Fan, M. Nakabayashi, Q. Li, L. Zhou, Q. Wang, C. Li, N. Shibata, K. Domen, Y. Li, Decoupling light absorption and carrier transport via heterogeneous doping in Ta_3N_5 thin film photoanode, Nat. Commun. 13 (2022) 7769.
[50] Y. Hu, Y. Pan, Z. Wang, T. Lin, Y. Gao, B. Luo, H. Hu, F. Fan, G. Liu, L. Wang, Lattice distortion induced internal electric field in TiO_2 photoelectrode for efficient charge separation and transfer, Nat. Commun. 11 (2020) 2129.
[51] Q. Meng, B. Zhang, L. Fan, H. Liu, M. Valvo, K. Edstrom, M. Cuartero, R. de Marco, G.A. Crespo, L. Sun, Efficient $BiVO_4$ photoanodes by postsynthetic treatment: remarkable improvements in photoelectrochemical performance from facile borate modification, Angew. Chem. Int. Ed. 58 (2019) 19027−19033.
[52] M. Zhang, F. Li, D. Benetti, R. Nechache, Q. Wei, X. Qi, F. Rosei, Ferroelectric polarization-enhanced charge separation in quantum dots sensitized semiconductor hybrid for photoelectrochemical hydrogen production, Nano Energy 81 (2021) 105626.
[53] W. Bai, Y. Zhou, G. Peng, J. Wang, A. Li, P.F.-X. Corvini, Engineering efficient hole transport layer Ferrihydrite-MXene on $BiVO_4$ photoanodes for photoelectrochemical water splitting: Work function and conductivity regulated, Appl. Catal., B 315 (2022).
[54] H. Zhang, D. Li, W.J. Byun, X. Wang, T.J. Shin, H.Y. Jeong, H. Han, C. Li, J.S. Lee, Gradient tantalum-doped hematite homojunction photoanode improves both photocurrents and turn-on voltage for solar water splitting, Nat. Commun. 11 (2020) 4622.
[55] G. Yang, Y. Li, H. Pang, K. Chang, J. Ye, Ultrathin cobalt−manganese nanosheets: An efficient platform for enhanced photoelectrochemical water oxidation with electron-donating effect, Adv. Funct. Mater. 29 (2019) 1904622.
[56] S. Zhang, Z. Liu, M. Ruan, Z. Guo, L. E, W. Zhao, D. Zhao, X. Wu, D. Chen, Enhanced piezoelectric-effect-assisted photoelectrochemical performance in ZnO modified with dual cocatalysts, Appl. Catal. B Environ. 262 (2020) 118279.
[57] L. Chen, Y. Xu, B. Chen, In situ photochemical fabrication of CdS/g-C_3N_4 nanocomposites with high performance for hydrogen evolution under visible light, Appl. Catal., B 256 (2019) 117848.
[58] G. Zhang, Y. Xu, M. Rauf, J. Zhu, Y. Li, C. He, X. Ren, P. Zhang, H. Mi, Breaking the limitation of elevated coulomb interaction in crystalline carbon citride for visible and near-Infrared light photoactivity, Adv. Sci. 9 (2022) 2201677.
[59] Y. Zheng, Q. Ruan, J. Ren, X. Guo, Y. Zhou, B. Zhou, Q. Xu, Q. Fu, S. Wang, Y. Huang, Plasma- assisted liquid-based growth of g-C_3N_4/Mn_2O_3 p-n heterojunction with tunable valence band for photoelectrochemical application, Appl. Catal., B 323 (2023) 122170.
[60] J. Zhang, Y. Zou, S. Eickelmann, C. Njel, T. Heil, S. Ronneberger, V. Strauss, P.H. Seeberger, A. Savateev, F.F. Loeffler, Laser-driven growth of structurally defined transition metal oxide nanocrystals on

Please cite this article as: M. Ai et al., Piezoelectric-enhanced n-TiO_2/$BaTiO_3$/p-TiO_2 heterojunction for highly efficient photoelectrocatalysis, Green Energy & Environment, https://doi.org/10.1016/j.gee.2023.12.001

carbon nitride photoelectrodes in milliseconds, Nat. Commun. 12 (2021) 3224.

[61] F. Wang, Q. Ding, J. Ding, Y. Bai, H. Bai, W. Fan, Frustrated Lewis pairs boosting photoelectrochemical nitrate reduction over $ZnIn_2S_4/BiVO_4$ heterostructure, Chem. Eng. J. 450 (2022) 138260.

[62] M. Zhang, J. Wang, H. Xue, J. Zhang, S. Peng, X. Han, Y. Deng, W. Hu, Acceptor-Doping Accelerated Charge Separation in Cu_2O Photocathode for Photoelectrochemical Water Splitting: Theoretical and Experimental Studies, Angew. Chem. Int. Ed. 59 (2020) 18463–18467.

Please cite this article as: M. Ai et al., Piezoelectric-enhanced n-TiO_2/$BaTiO_3$/p-TiO_2 heterojunction for highly efficient photoelectrocatalysis, Green Energy & Environment, https://doi.org/10.1016/j.gee.2023.12.001